J Geod (2006) 80: 591–607
DOI 10.1007/s00190-006-0078-0

ORIGINAL ARTICLE

J.-M. Nocquet · P. Willis · S. Garcia

Plate kinematics of Nubia–Somalia using a combined DORIS and GPS solution

Received: 15 February 2006 / Accepted: 17 June 2006 / Published online: 26 September 2006

Abstract We have used up to 12 years of data to assess DORIS performance for geodynamics applications. We first examine the noise characteristics of the DORIS time-series of weekly station coordinates to derive realistic estimates of velocity uncertainties. We find that a combination of white and flicker noise best explains the DORIS time-series noise characteristics. Second, weekly solutions produced by the Institut Géographique National/Jet Propulsion Laboratory (IGN/JPL) DORIS Analysis Centre are combined to derive a global velocity field. This solution is combined with two independent GPS solutions, including 11 sites on Nubia and 5 on the Somalia plate. The combination indicates that DORIS horizontal velocities have an average accuracy of 3 mm/year, with best-determined sites having velocity accuracy better than 1 mm/year (one-sigma levels). Using our combined velocity field, we derive an updated plate kinematics model with a focus on the Nubia–Somalia area. Including DORIS data improves the precision of the angular velocity vector for Nubia by 15%. Our proposed model provides robust bounds on the maximum opening rates along the East African Rift (4.7–6.7 mm/year). It indicates opening rates 15 and 7% slower than values predicted by NUVEL-1A for the southern Atlantic Ocean and Indian Ocean, respectively. These differences are likely to arise from the fact that NUVEL-1A considered Africa as a single non-deforming plate, while here we use a more refined approach.

Keywords Africa · Nubia · Somalia · Plate motion · DORIS · GPS · Terrestrial reference frame · Plate tectonics · NUVEL-1A

J.-M. Nocquet (✉) · S. Garcia
UMR6526 Géosciences, Azur, 06560 France
E-mail: nocquet@geoazur.unice.fr
E-mail: sebastian.garcia@dstu.univ-montp2.fr
Tel.: +33-4-92942625
Fax: +33-4-92942610

P. Willis
Institut Geographique National, Direction Technique, 2 avenue Pasteur, BP 68, 94160 Saint-Mande, France

P. Willis
Jet Propulsion Laboratory, California Institute of Technology, 4800 Oak Grove Drive, Pasadena, CA 91109, USA
E-mail: Pascal.R.Willis@jpl.nasa.gov
Tel.: +1-818-3934748
Fax: +1-818-3934965

1 Introduction

About two decades separates the onset of the plate tectonics theory (Wilson 1965; McKenzie and Parker 1967; Morgan 1968; Le Pichon 1968) to the first direct measurement of plate motion using space-geodetic techniques. During those two decades, kinematics of plates could only be derived using indirect and partial measurements, mainly limited to diverging oceanic plate boundaries. Moreover, deriving relative plate motion from mid-ocean ridge spreading rates inferred from magnetic lineations assumed that (1) measurements made at diverging oceanic boundaries could be extrapolated to the rest of the plate so that the motion could be explained by a single rotation vector; (2) plate motions remain steady over the period used to correlate the magnetic anomalies (3.16 Ma for NUVEL-1A); (3) the magnetic inversion's time-scale is perfectly calibrated (DeMets et al. 1994). Finally, in the early years of the plate tectonics theory, although it was recognised that rigidity of plate was an idealization, the level of validity of such an assumption was unknown (Gordon 1995). Geology-based global kinematic models had to assume that the plates were rigid and could confirm it a posteriori through plate circuit closures. However, this verification was indirect as non-closure could imply non-rigidity of plates as well as errors in the data used for an individual plate-pair motion.

Space-geodetic techniques achieved the accuracy to detect the present-day motion of tectonics plate in the mid-1980s (e.g. Christodoulidis et al. 1985; Herring et al. 1986). In the early 1990s, the first space-based geodetic plate kinematic models, using only a few years of data, were proposed (e.g. Cretaux et al. 1998) and showed a surprisingly good agreement with geological models' averaged motion over several

million years, e.g. NUVEL-1 (DeMets et al. 1990). However, as both the spatial coverage of geodetic sites on the Earth's surface and their accuracy increased, several discrepancies in plate motions have been found between space-geodetic and geological estimates (DeMets 1995; Argus and Heflin 1995; Larson et al. 1997; Kreemer et al. 2003). Whether such discrepancies reflect recent changes in kinematics or biases in one or both types of data still remains an important question that requires a careful analysis of the error budgets (Calais et al. 2003).

Among the major plates, Africa has long-resisted investigation due to the lack of geodetic measurements. While both seismological and geomorphological observations clearly indicate that the African continent is breaking apart along the East African Rift (EAR) into two sub-plates (Nubia plate west of the EAR and Somalia plate east of the EAR), DeMets et al. (1990) were unable to resolve separate Nubia and Somalia plates and therefore treated the two plates as a single Africa plate. Eventually, Jestin et al. (1994) and Chu and Gordon (1999) were able to discriminate the motion of the two plates using magnetic anomalies along the southwestern Indian ridge. Until very recently, the Antarctic plate had more permanent GPS sites than the Africa plate. As a consequence, even the most recent geodesy-based kinematics model (Sella et al. 2002; Prawirodirdjo and Bock 2004) used only four and five sites, respectively, to determine the kinematics of Nubia and only two and three sites, respectively, for Somalia.

In this study, we combine one DORIS plus two global GPS solutions to derive plate motion based on 16 sites for the Nubia plate and 5 sites for the Somalia plate. We use the derived velocity field to estimate the motion of the two plates relative to their neighbouring plates and compare them to the previous estimates from NUVEL-1A and other recently published plate kinematic models.

2 Input data

2.1 IGN/JPL DORIS analysis

We include DORIS data (Fig. 1) processed at the Jet Propulsion Laboratory (JPL) using GIPSY/OASIS software (Webb and Zumberge 1995; Willis et al. 2005a). All DORIS/Doppler data available at the International DORIS Service (IDS) (Tavernier et al. 2005) data centre at NASA/CDDIS (National Aeronautics and Space Administration / Crustal Dynamic Data Information System) were processed from January 1993 to August 2005 on a daily basis in a multi-satellite mode (Willis et al. 2003, 2005a).

We excluded all DORIS/Jason-1 data due to an unexpected sensitivity of the on-board ultra-stable oscillator (USO) to radiation when crossing the South Atlantic Anomaly (SAA) (Willis et al. 2004). Also, we did not use DORIS/SPOT-4 for 1998 due to an error in the pre-processing of the phase centre correction of these data (Willis et al. 2006b). We later found that this error was recoverable by re-computing the correct satellite phase centre correction, but was not included here. DORIS/SPOT-4 data for 1998 will be available in our future solutions.

We use the latest available solutions based on the recent Gravity Recovery And Climate Experiment (GRACE)-derived GGM01C gravitational field model (Tapley et al. 2004) up to degree and order 120, which leads to a significant improvement in the DORIS results (Willis and Heflin 2004). Indeed, the DORIS technique uses low-Earth orbiting (LEO) satellites (830 km altitude orbits for SPOT satellites, 1,300 km for TOPEX/Poseidon and Jason-1 satellites) and is therefore very sensitive to any gravitational field mismodelling.

DORIS data are processed routinely on a daily basis using a free-network approach (also called a fiducial-free approach, Heflin et al. 1992). The daily solutions (station coordinates) are then combined together to form weekly solutions (Willis et al. 2005a). These weekly solutions are posted at the IDS NASA/CDDIS data centre (ftp://cddis.gsfc.nasa.gov/pub/doris/products/sinex_series/ignwd) either as free-network solutions or projected solutions (Sillard and Boucher 2001), directly expressed in ITRF2000 (Altamimi et al. 2002). Both time-series are available in SINEX format and are posted regularly within 24 h after data availability at NASA/CDDIS data centre, with specific documentation (weekly summary reports), describing the data used or rejected per station and per satellite.

For the projected/transformed weekly time-series (ignwd04), the most important information contained in the SINEX format is also duplicated in a different format, providing per station (i.e. one file per station) the coordinate differences expressed in ITRF2000 with regards to a fixed a priori position (no velocity correction). These differences are provided in Cartesian *X, Y* and *Z* and also in East, North and Vertical with formal errors, but without the full covariance information. This format is called STCD (STation Coordinate Differences) and weekly time-series are regularly updated and available at ftp://cddis.gsfc.nasa.gov/pub/doris/products/stcd/ign03wd01.

We base our initial analysis of DORIS noise on the IGN/JPL STCD files. However, the current STCD files posted at NASA/CDDIS may present a problem when multiple DORIS stations have observed at the same DORIS site (typically after a change in equipment), because their a priori positions in the STCD files is selected independently and may not be compatible with the DORIS–DORIS geodetic local ties between these stations. Due to operational considerations, it is not currently possible to do so, as the STCD files are continuously updated (result of the last processed week is added to the end of the STCD file, using always the same a priori position as provided in the file) and as the local geodetic tie information (3D vectors between successive DORIS antenna and their precisions) may only be available a long time after the first observations and weekly results.

The geodetic local ties are provided by the IGN/SIMB (Fagard 2006), which is in charge of the installation and the maintenance of the DORIS tracking network, and may change with time, due to the availability of a new

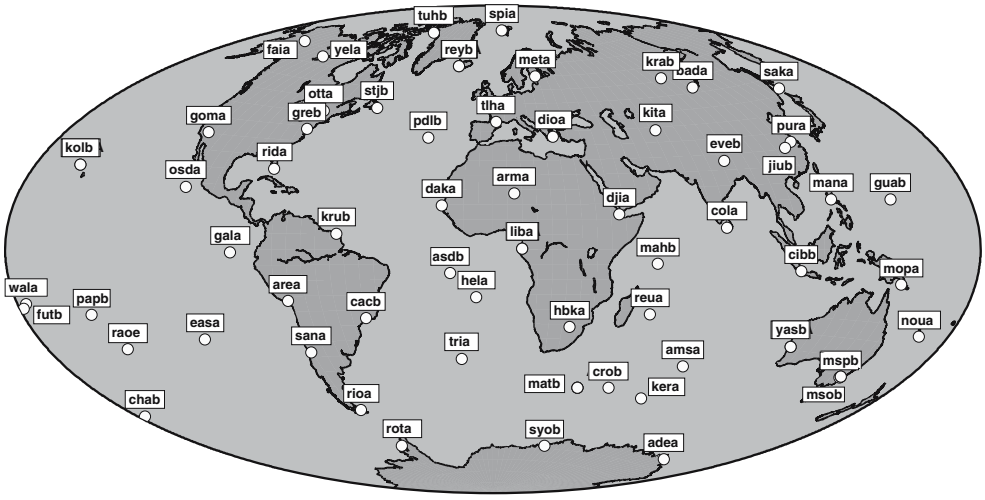

Fig. 1 DORIS sites used in the study (1993.0–2005.5). Acronyms used on the map correspond to the name of the first DORIS beacon installed at the site and used in the DORIS data files and for naming the corresponding Station Coordinate Differences (STCD) file

terrestrial-geodetic survey. To solve this operational problem (i.e. multiple DORIS occupation of the same site leading to possible inconsistencies in different STCD files), we have kept unchanged the STCD file of the most recent occupation and modified the file of any previous occupation to ensure that the vector between the a priori coordinates of any two stations in the STCD files is exactly identical to the local tie provided by the IGN/SIMB. The obtained time-series for a few sites relevant for the present study are displayed in Fig. 2.

In a second step, we combined all the DORIS weekly free-network solutions, including DORIS–DORIS geodetic local tie information with proper weighting (formal errors also provided by IGN/SIMB), as well as tight constraints between station velocities at the same site, except for stations that do not have a continuous velocity over time, such as Arequipa due to the nearby 2001 Mw=8.3 earthquake (Willis and Ries 2005). We have also introduced several discontinuities for station coordinates as suggested by several authors (Willis and Ries 2005; Soudarin 2005, IDS Analysis Forum) and summarized by Willis et al. (2005b) for preparation of the next release of the International Terrestrial Reference Frame (ITRF2005, Altamimi et al. 2006). Our own selection of DORIS station discontinuities is presented in Table 1.

This DORIS free-network cumulative solution (Willis et al. 2005a) was then projected (Sillard and Boucher 2001) and transformed into ITRF2000 through a 14-parameter Helmert transformation to provide coordinates and velocities in ITRF2000 (Fig. 3) using full covariance information, and based on the complete DORIS data set. In that solution, the full variance–covariance (VCV) matrix was rescaled, directly using the reduced χ^2 derived from the weekly free-network solutions' combination. In the present study, this cumulative solution with its full rescaled VCV matrix (designed hereafter as the IGN05D02 solution) is used as input to the GPS/DORIS combination solution.

2.2 GPS solution

Our GPS solution (designated hereafter as the GEOAZUR-AFRC solution, see Fig. 4) includes data from 1998.0 to 2005.3 at 65 global continuous GPS (cGPS) sites, mainly from the International Global Navigation Satellite Systems (GNSS) Service (IGS) network (Beutler et al. 1999; Moore and Neilan 2005). The solution is denser in Africa and its surroundings using also data from UNAVCO (PLHW, Egypt and LAUG, Lebanon, ftp data-put.unavco.org) and the Commissariat à L'Energie Atomique (ALEX, Egypt). The GEOAZUR-AFRC solution was produced using the GAMIT/GLOBK software version 10.20 (King and Bock 2005).

Our analysis strategy uses double-differenced GPS carrier-phase measurements to estimate daily station coordinates, satellite state vectors, seven tropospheric delay parameters per site and per day, horizontal tropospheric gradients and carrier-phase ambiguities. We used IGS final orbits and applied absolute elevation-dependent antenna phase centre models following the tables recommended by the IGS, solid Earth and polar tide corrections following the 2003 IERS conventions (McCarthy and Petit 2004) and ocean loading corrections using the CSR4.0 ocean tide model (Eanes and Schuler 1999).

To minimize processing time, we divided the whole GPS network into a global network of 50 sites and a densified regional network covering Africa and its surrounding 30 sites, sharing 15 of them with the global network. In a first step, the daily solutions of the two networks were combined and 14-parameter transformed into ITRF2000 to produce time-series of station coordinates. Outliers and jumps in the time-series are detected and corrected by estimating the offset. We also use the time-series to estimate site-specific parameters for a noise model that includes white and random-walk processes. In a second step, we combine the daily loose solutions

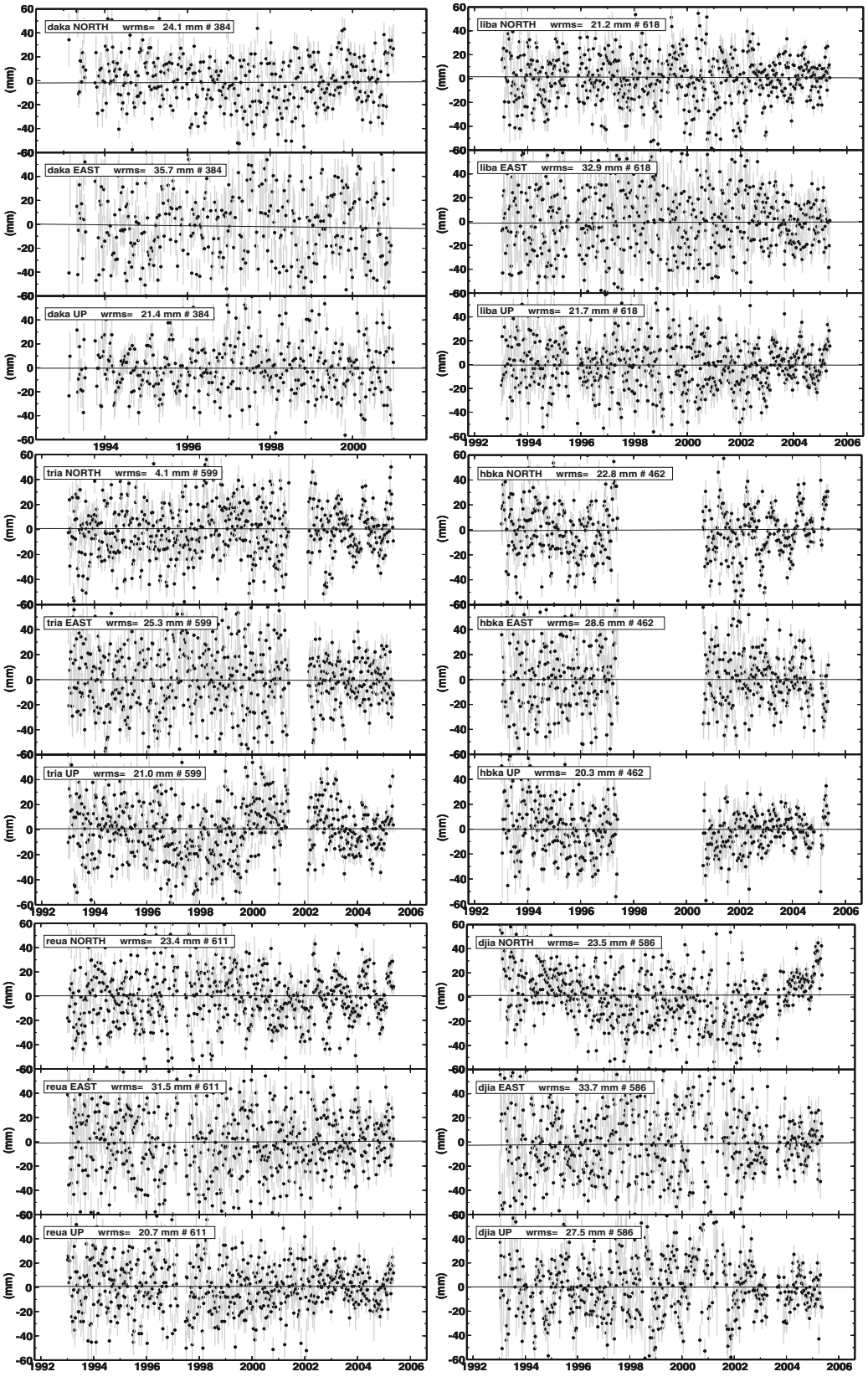

Fig. 2 Detrended (velocity removed) time-series for four DORIS sites on the Nubia plate (daka, tria, liba, hbka) and Somalia plate (reua, djia). *Numbers after hash* indicate the number of weekly solutions available for each site

Table 1 Discontinuities considered (Pos = position, Vel = velocity) when combining DORIS weekly free-network solution into cumulative solution (Pos and Vel) IGN05D02

Acronym	Station	λ	φ	Epoch	Pos	Vel	Comment
COLA	Colombo	79.87	6.88	16-NOV-1994	X		Earthquake
DIOA	Dionysos	23.93	38.07	01-APR-1995	X		
EASA	Easter Island	−108.62	−26.87	12-FEB-1998	X		
EVEB	Everest	86.87	27.95	23-JAN-2003	X		
FAIB	Fairbank	−146.48	64.97	03-NOV-2002	X	X	Earthquake
KESB	Kerguelen	70.25	−48.65	31-MAR-2004	X		
KRAB	Krasnoyarsk	92.78	55.98	01-JAN-1999	X		
MANB	Manilla	121.03	14.53	01-JAN-2005	X	X	Human intervention
MARB	Marion Island	37.85	−45.12	01-JAN-2003	X		
ROTA	Rothera	−67.88	−66.43	20-FEB-1997	X	X	
SAKA	Sakhakinsk	142.72	47.02	10-OCT-1994	X		
SAKA	Sakhakin	142.72	47.02	25-NOV-2001	X		
SODB	Soccorro Island	−109.05	18.73	03-OCT-2002	X		
STJB	St John	−51.32	47.58	27-AUG-2002	X	X	
TRIB	Tristan da Cunha	−11.68	−36.93	31-JUL-2004	X		Earthquake

λ, φ: longitude and latitude of sites in decimal degrees. Most discontinuities are still unexplained; see Willis and Ries (2005) for additional discussion

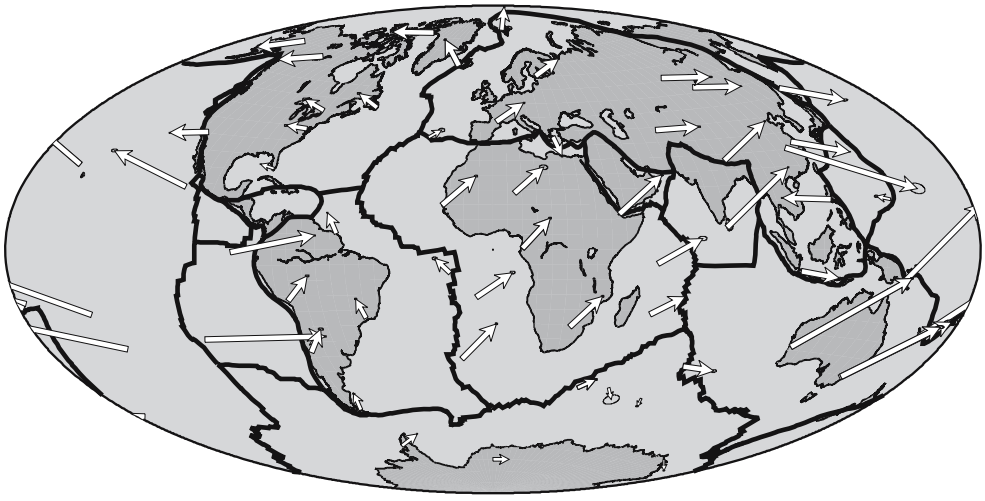

Fig. 3 DORIS-derived velocities expressed in ITRF2000 from the IGN05D02P cumulative solution. For the sake of clarity, sites with poorly determined velocities are not represented. *Black lines* indicate major tectonic plates boundaries used in the NUVEL-1 model

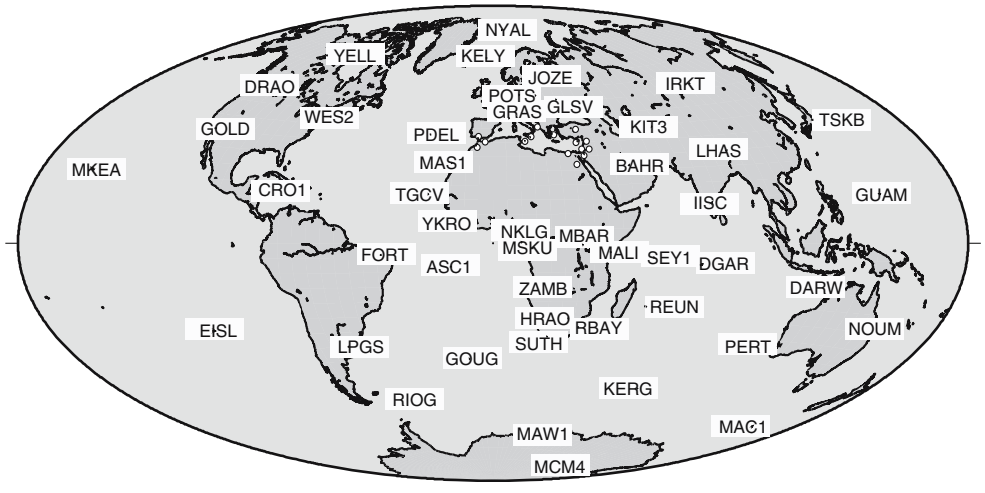

Fig. 4 cGPS sites included in the GEOAZUR-AFRC solution. For the sake of clarity, sites in the Mediterranean are represented with *white dots* only

to produce a loosely constrained position–velocity solution. Minimal constraints (Sillard and Boucher 2001) are then applied to the VCV matrix.

Besides the cGPS sites, our solution also includes a campaign site located on the Island of Madagascar (MIR1) within the Somalia plate. The site was observed during 2 weeks in 1998 and 3 days in 2004. The data were included in the processing of our global network. Repeatabilities for the 1998 campaign are 2.2 and 5.0 mm (north and east component, respectively) and 2.2 and 3.4 mm for the 2004 campaign (north and east component, respectively). The MIR1 velocity standard deviation in our global solution is 0.5 mm/year before combination.

3 Combination of DORIS and GPS velocity field solutions

3.1 Methodology

A rigorous combination methodology enables us to derive a single, consistent, extensive and accurate velocity field from heterogeneous solutions coming from different geodetic techniques. It provides a way to assess the solutions' quality, by cross-checking position and velocities in each individual solution, and therefore enables the detection of outliers. By averaging down random and systematic errors associated with processing strategies and techniques, it provides a robust resulting solution including information available.

We use the combination algorithm developed by Altamimi et al. (2002) that was used to derive ITRF2000. Our input data are two GPS solutions GeoAZUR.AFRC and the IGS weekly combined solution IGS06P01 (Ferland et al. 2000) and the DORIS solution IGN05D02. All three are minimally constrained solutions. The combination involves simultaneously estimating, for each site i in solution s (s = IGN05D02, GEOAZUR-AFRC, IGS06P01), the velocity V^i_{comb}, and a 14-parameter transformation between the individual and the combined solution using:

$$\begin{aligned} X^i_s &= X^i_{\text{comb}} + (t^i_s - t_0)V^i_{\text{comb}} \\ &+ T_k + D_k X^i_{\text{comb}} + R_k X^i_{\text{comb}} \\ &+ (t^i_s - t_k)\left[\dot{T}_k + \dot{D}_k X^i_{\text{comb}} + \dot{R}_k X^i_{\text{comb}}\right], \end{aligned} \quad (1)$$

$$V^i_s = V^i_{\text{comb}} + \dot{T}_k + \dot{D}_k X^i_{\text{comb}} + \dot{R}_k X^i_{\text{comb}}, \quad (2)$$

where X^i_s is the position of site i in solution s at epoch t^i_s, X^i_{comb} the estimated position of site i at epoch t_0. T_k, D_k, R_k and $\dot{T}_k$, $\dot{D}_k$, $\dot{R}_k$ are the transformation parameters between individual solutions s and the combined solution and their time derivatives, respectively. t^i_s is the epoch of minimal position variance for the solution s, which is generally the mid-point of the observation time-span included in the solution, when observation precision is constant in time. t_k is the epoch of reference (conventional choice) of the transformation parameters.

The reference frame (ITRF2000) is applied in the combination by imposing minimal constraints to the combined solution using a subset of best-determined ITRF2000 sites (velocity standard deviation smaller than 1 mm/year on each component), realising a global coverage. The strength of the combination relies on the ties between GPS and DORIS markers. In the present combination, 61 DORIS–GPS ties (all provided by IGN/SIMB) (Fagard 2006) were included as geocentric 3D Cartesian vectors with their proper variance. We imposed that the velocity be the same at co-located DORIS and GPS sites. We validated the geodetic local ties in the combination by carefully checking the changes in residuals before and after adding the ties and velocity constraints. In a few cases, like in Hastebeeshoek (HRAO, harb), we had to loosen the constraints when high residuals (> 3 mm/year) were found.

3.2 Weighting of individual solutions

One key point of the combination consists in assigning a realistic full VCV matrix to the individual input solutions. Ideally, such a VCV matrix should reflect both realistic estimates of positions and velocities and of the correlation between both coordinates components and inter-site positions and velocities. Two end-member techniques currently exist to produce realistic uncertainties. In a time-series approach, the noise content of daily/weekly position is analysed to simultaneously obtain the level of the chosen model of noise, the velocities and their uncertainties, possibly also solving for annual and semi-annual signals.

Using this approach, several groups (Zhang et al. 1997; Mao et al. 1999; Williams et al. 2004) have clearly demonstrated the presence of time-correlated (coloured) noise in GPS time-series. They showed that assuming that only white noise is present in the time-series led to underestimating velocity uncertainties by up to an order of magnitude. Williams and Willis (2006) analysed a subset of 31 DORIS time-series using the maximum likelihood estimation (MLE) algorithm described in Williams (2003). They conclude that a combination of both flicker and variable white noise best explain the DORIS time-series as a whole. They found an average ratio of three between the uncertainties derived assuming white noise only to that obtained using their best-fit model.

Here we performed a similar analysis on a selection of 74 DORIS time-series for the sites that were included in our combination. While a model including flicker and white noise is preferred for a majority of sites, a significant part of sites ($\sim$40%) have a preferred model including white plus random-walk noise. A fractional integer spectral index analysis leads to a mean value of $\kappa = -1.5$, confirming that noise characteristics for DORIS time-series have a behaviour lying between white plus flicker noise and white plus random-walk noise.

In this study, the mean level of this white noise is found to be, respectively, 24.3, 27.7 and 25.0 mm in the north, east and vertical components. The mean level of flicker noise is

found to be, respectively, 18.7, 24.5 and 10.9 mm/yr$^{1/4}$ in the north, east and vertical components. This analysis indicates that the best-determined component is often the vertical and the worst the east component, a result confirmed by the combination results (see below), and previously discussed by other authors (Soudarin et al. 1999; Willis et al. 2006a, Williams and Willis 2006).

As a third test, we compare the standard deviations of the velocities taken from the IGN05D02 solution to the ones derived from the MLE algorithm for the white plus flicker noise model. We find good agreement between the standard deviations of the velocities included in the IGN05D02 (reweighted) with uncertainties derived from the MLE algorithm: the average ratio between the two is 0.96 for the east component, 1.42 for the north component, indicating that, on average, the variance rescaling applied to the solution IGN05D02, using the χ^2 value of the combination of individual weekly solutions, correctly accounts (on average) for noise characteristics in velocity uncertainty estimates.

While a time-series approach provides velocity uncertainties by accounting for noise characteristics of the position time-series, the analysis is made for each site and for each component separately. It therefore neglects any correlations between site components, as well as inter-site components. As an alternative attempt to correctly assess DORIS solution VCVs, we use an iterative Helmert block algorithm (Altamimi et al. 2002) to rescale the variance of individual solution during the combination process.

In this approach, an a posteriori variance factor σ_0^S is calculated for each individual solution at the same time as the other parameters. The obtained σ_0^S is then used as a scaling factor applied to each individual VCV matrix. The procedure is performed iteratively until both individual and the global a posteriori variance factors equal unity. The formula for σ_0^S is given in Altamimi et al. (2002, Eqs. A16 and A17). For an individual solution s, σ_0^S basically indicates if the agreement at sites shared by several solutions (or where a tie is available) is consistent with the formal error. This number is therefore a useful external indicator of the accuracy of an individual solution and technique if the combination involves different techniques.

For the present combination, we obtain a variance-scaling factor of 5.6 for the IGN05D02 DORIS solution and 8.5 for the GEOAZUR-AFRC GPS solution and 5.2 for the IGS06P01 GPS solution. These results suggest that the time-series analysis provides velocity uncertainties that still underestimate the true accuracy.

3.3 Statistics of the combination and quality assessment of DORIS solution

The result of the combination is a SINEX file including the full VCV matrix in which positions and velocities are expressed in ITRF2000. The level of agreement between solutions, given by the weighted root mean square (WRMS) is shown in Table 2. For the horizontal velocity components, the WRMS is of the order of 0.5 mm/year for the GPS solutions and 3 mm/year for the DORIS solution. Best-determined sites for the DORIS solution have horizontal velocities uncertainties of 1 mm/year or slightly better (1σ) and correspond to DORIS stations with the longest time span of observations.

In the DORIS solution, the vertical component is usually the best-determined component, as indicated in the combination by a smaller WRMS. On the contrary, for the GPS solutions, horizontal velocity components are on average two times better determined than the vertical velocities. The fact that the DORIS-derived vertical component is as good as the horizontal components and in general better than the east was mentioned earlier by several authors (Soudarin et al. 1999; Willis et al. 2006a) and is usually attributed to the DORIS use of the SPOT's sun-synchronous satellite having almost polar orbits.

Best-determined DORIS sites have vertical uncertainties of 0.7 mm/year, which make this technique comparable with GPS and potentially well-suited for long-term monitoring of tide-gauges and global sea level (cf. Nerem and Mitchum 2002; Morel and Willis 2002).

4 Kinematics of Nubia

We first start our velocity field analysis (Table 3) by solving for a rigid rotation for sites located west of the EAR (Nubia plate). We use the methodology of Nocquet et al. (2001) to find the subset of sites that best defines the motion of rigid Nubia in the ITRF2000 frame. This methodology takes into account the full VCV matrix in the rotation vector estimation, uses minimum variance and χ^2 criterions to select the subset of sites that provides the best estimation. It also uses F-ratio, Student and χ^2 tests to detect outliers.

We find that the best estimate of the Nubia rotation vector is obtained using a subset of 16 sites including the ALEX, GMAS, GOUG, MAS1, NKLG, PHLW, TGCV, SUTH, SUTM, YKRO, ZAMB GPS sites together with the daka, hela, liba, tria DORIS sites and HRAO(D) as a GPS–DORIS co-located site. A reduced χ^2 of 1.5 indicates an overall good agreement between formal errors and residual velocities. The WRMS of residual velocities is 0.7 mm/year, a value typically found in other stable plate interiors (e.g. Nocquet et al. 2005; Calais et al. 2005).

The largest residuals are found for ALEX (Alexandria, Egypt) and ZAMB (Lusaka, Zambia) and are $\sim$1.6 mm/year. While a χ^2 test rejects ALEX at a 95% confidence level, both F-ratio and Student tests fail to indicate significant velocity discrepancy with the overall motion of Nubia. We therefore included ALEX in our calculation of the Nubia angular velocity vector. MSKU is rejected by all tests as found in earlier studies (e.g. Nocquet and Calais 2004).

Previously published studies used at most nine sites (Fernandes et al. 2004) to determine the Nubia plate kinematics, mostly in South Africa, Gough Island and the northwestern coast of the African continent. Our solution samples both the oceanic (five sites) and continental (nine sites) lithosphere

Table 2 WRMS of individual solutions obtained in the combination

Solution	WRMS horizontal (mm)	WRMS vertical (mm)	WRMS horizontal (mm/year)	WRMS vertical (mm/year)	Scaling factor
IGN05P02D	21.9	15.0	3.1	1.9	5.6
GEOAZUR-AFRC	1.6	2.4	0.4	0.7	8.5
IGS06P	1.8	4.0	0.6	1.0	5.2

Scaling factor is the factor applied to the variance of individual solutions as found by the Helmert blocking algorithm

of the Nubia plate and includes sites in Egypt thus realising an optimal coverage of Nubia. Compared to previous studies, it includes longer time-series providing better velocity estimates. The quality of our pole determination is reflected in the variance of the pole, the most precise published so far.

The DORIS solution contributes to the determination of the Nubia plate kinematics in two different ways: sites like Hartebeesthoek (HRAO) in South Africa benefit from the DORIS velocity. However, the relative weight between GPS and DORIS solution makes the contribution to the determination of the velocity small for this site. DORIS-only sites included in the estimation are tria and hela (Tristan Da Cunha Island, Saint Helen island, southern Atlantic), liba (Libreville, Gabon, Central Africa) and daka (Dakar, Senegal, Western Africa).

The WRMS for these sites is 1.3 mm/year, only slightly higher than the WRMS obtained for the best-determined GPS sites. The quality of the determination of a plate rotation vector is a function of: (1) the geometry realised by the sites sampling the plate; and (2) the precision of the site velocities, which includes the level of residuals if the pole variance is rescaled by the reduced χ^2. We therefore can estimate the contribution of DORIS sites in the determination of the kinematics of the Nubia plate by removing the DORIS sites in the estimation and looking at the plate rotation vector changes in both value and variance.

Removing the DORIS sites insignificantly changes the calculated pole ($< 0.1°$ in position $< 0.001°$/Myear in angular velocity), but the variance increases by 15%. With two sites located on the oceanic part of the plate (Tristan Da Cunha and Saint Hellen islands), DORIS solution, together with the GPS sites located at Gough Island, Cape Verde and Canaries islands, helps to ensure that the oceanic and continental lithosphere forms a single, rigid Nubia plate.

5 Kinematics of Somalia and the East African Rift opening rate

Figure 5 shows the residual velocities in a Nubia-fixed reference frame. It clearly indicates eastward residual motion for sites located east of the EAR. MBAR is surrounded by the western and eastern branch of the rift and belongs to a possible independent Victoria plate (Ebinger 1989; Calais et al. 2006). It can therefore not be used to determine the Somalia plate kinematics. Previous GPS-derived Somalia/Nubia kinematics estimates by Sella et al. (2002), Fernandes et al. (2004) and Prawirodirdjo and Bock (2004) only used 2–4 sites to estimate the kinematics of the Somalia plate.

With such a small number of available sites, any millimetre per year error in the velocity determination at one of the sites will strongly impact the pole determination and the predicted opening rates along the EAR. For instance, the IGS cumulative solution that we included in the combination shows a lengthening rate of the baseline between MALI and SEY1 at a rate 2.27 ± 0.43 mm/year, not consistent with a rigid plate assumption, while our GEOAZUR-AFRC GPS solution finds a lengthening rate of 0.92 ± 0.90 mm/year, not significant at the 95% confidence level.

The combination indicates that the difference mostly arises in a difference found at SEY1 in the two solutions. Inverting a Somalia plate rotation vector separately using the GEOAZUR-AFRC provides significantly smaller residuals than including the IGS06P01 solution. Sella et al. (2002) had already noticed a possible problem with the SEY1 time-series and excluded its 1995–1996 data from their solution. We therefore suspect that the difference between the GEOAZUR-AFRC and IGS cumulative solution arises from the fact the latter includes early data for SEY1, while the GEOAZUR-AFRC only includes data after 1998.0. We therefore rejected SEY1 from the IGS solution before the combination.

Our calculated rotation vector for Somalia is based on five sites. Among them, REUN is located on a volcanic island. Any volcanic-related deformation may impact the REUN velocity and therefore bias our Somalia rotation vector estimate. Similarly, the main boundary between Nubia and Somalia south of latitude 20°S becomes diffuse, as relative motion between the two plates becomes smaller. RBAY could therefore belong to any of the two plates or to the deformation zone.

In order to assess the sensitivity of our calculated rotation vector for Somalia to the chosen sites, we perform a simple robustness test: we successively remove one and then two sites from the (MALI, MIR1, RBAY, REUN, SEY1) subset and calculate new rotation vectors. The so-obtained Euler poles are shown in Fig. 5. The scatter of the different calculated Euler pole is large ($\sim 25°$ in longitude). However, the latitude of the Euler pole and the angular velocities are highly correlated parameters in the least-squares inversion and smaller angular velocity may compensate an Euler pole located more southward. The comparison has therefore to be made on the predicted velocities along the EAR. In Northern Ethiopia (longitude 41°E, latitude 10°N), where the rate is expected to be the largest of the EAR, the model prediction

Table 3 ITRF2000 velocities of sites in the combined solution and used to derive the plate motion; associated one-sigma errors and residual velocities with respect to the plate the site belongs

Site	λ	φ	V_e	V_n	σ_{Ve}	σ_{Vn}	Res_V_e	Res_V_n
Antarctica (anta)								
CAS1	110.52	−66.14	2.44	−9.84	0.17	0.16	−0.46	0.43
CRAR	166.67	−77.77	9.61	−11.04	1.57	1.93	0.16	−0.20
DAV1	77.97	−68.45	−1.67	−5.75	0.18	0.16	0.55	−0.40
MAW1	62.87	−67.47	−3.05	−3.15	0.19	0.15	−0.29	−0.79
MCM4	166.67	−77.76	9.12	−11.40	0.16	0.15	−0.33	−0.56
SYOG	39.58	−68.88	−3.36	1.89	0.35	0.40	−0.03	−0.58
VESL	−2.84	−71.56	−0.41	9.07	0.40	0.44	−0.46	−0.66
adea	140.00	−66.52	9.11	−11.66	0.56	0.54	0.99	0.32
syob	39.58	−68.88	−4.66	1.74	1.00	0.87	−1.33	−0.73
KERG_D	70.26	−49.16	5.46	−3.56	0.15	0.10	0.24	0.30
Arabia (arab)								
BAHR	50.61	26.06	31.44	27.97	0.14	0.09	0.17	0.13
YIBL	56.11	22.05	36.36	30.79	1.96	1.75	2.59	2.47
Australia (aust)								
ALIC	133.89	−23.53	31.64	57.67	0.27	0.23	0.21	0.08
AUCK	174.83	−36.42	3.32	38.79	0.20	0.15	−1.29	−0.91
CEDU	133.81	−31.69	28.97	57.98	0.26	0.24	0.66	0.41
DARW	131.13	−12.76	35.16	56.65	0.22	0.14	−0.07	−1.17
HOB2	147.44	−42.61	13.88	55.24	0.17	0.14	−0.25	0.67
JAB1	132.89	−12.58	34.96	58.16	0.37	0.31	0.09	0.46
MOBS	144.98	−37.64	20.02	56.29	2.21	1.88	1.12	0.93
NNOR	116.19	−30.88	38.83	56.04	1.27	0.94	1.11	−0.55
NOUM	166.41	−22.14	20.00	45.54	0.22	0.15	−0.58	0.08
PERT	115.89	−31.63	38.81	56.67	0.15	0.10	1.04	0.15
STR1	149.01	−35.13	17.92	54.55	0.81	0.81	−0.31	0.48
STR2	149.01	−35.13	18.21	54.32	2.08	2.30	−0.02	0.26
TIDB	148.98	−35.22	17.86	54.65	0.17	0.13	−0.33	0.58
TOW2	147.06	−19.15	28.00	54.43	0.26	0.22	−0.61	−0.34
YAR1	115.35	−28.88	38.74	55.92	0.17	0.12	0.34	−0.49
YARR	115.35	−28.88	38.17	56.91	1.25	1.02	−0.23	0.50
yara	115.35	−28.88	38.94	56.03	1.57	1.14	0.53	−0.38
yasb	115.35	−28.88	38.94	56.03	1.57	1.14	0.53	−0.38
Eurasia (eura)								
GLSV	30.50	50.18	22.75	11.37	0.17	0.12	−0.21	0.33
ARTU	58.56	56.25	24.87	4.73	0.23	0.25	−0.11	0.18
BOR1	17.07	52.09	20.76	13.49	0.14	0.13	0.42	0.20
BRUS	4.36	50.61	17.91	14.06	0.14	0.13	−0.35	−0.71
GRAS	6.92	43.56	20.95	14.77	0.13	0.10	0.61	0.24
IRKJ	104.32	52.03	25.08	−7.96	1.42	1.85	0.37	−0.45
IRKT	104.32	52.03	24.14	−8.58	0.15	0.15	−0.57	−1.08
JOZE	21.03	51.91	21.38	13.03	0.14	0.12	0.28	0.33
JOZ2	21.03	51.91	21.21	12.17	1.72	2.23	0.12	−0.53
KOSG	5.81	51.99	18.26	14.76	0.85	0.99	0.06	0.13
KSTU	92.79	55.81	24.42	−5.75	0.28	0.28	−0.62	−1.13
LAMA	20.67	53.71	19.65	12.76	0.16	0.16	−0.98	0.00
LROC	−1.22	45.97	18.82	14.60	1.06	1.30	0.50	−0.58
MADR	−4.25	40.24	18.51	14.81	0.17	0.13	−0.58	−0.55
MDVJ	37.21	55.84	22.70	9.42	1.32	1.72	−0.13	−0.25
MDVO	37.22	55.85	23.01	11.62	0.31	0.33	0.17	1.95
METZ	24.40	60.05	19.90	11.58	1.52	2.07	0.12	−0.56
MOBN	36.57	54.93	23.48	10.13	0.95	1.26	0.55	0.32
MORP	−1.69	55.03	17.31	14.61	1.32	1.87	1.51	−0.60
NRIL	88.36	69.23	21.79	−3.13	0.31	0.36	−0.44	0.32
NVSK	83.24	54.66	26.07	−2.44	1.28	1.31	0.37	−0.35
NYA1	11.87	78.86	10.20	14.03	0.17	0.19	−0.94	0.07
OBE2	11.28	47.89	20.79	14.73	0.72	0.78	0.57	0.68
OBER	11.28	47.89	20.45	14.37	0.79	0.57	0.23	0.32
ONSA	11.93	57.22	17.36	13.58	0.13	0.12	−0.72	−0.38
OPMT	2.33	48.65	17.88	14.20	1.78	2.24	−0.47	−0.74
PENC	19.28	47.60	22.97	13.18	0.30	0.35	1.29	0.21
POLV	34.54	49.41	22.88	10.79	0.91	1.21	−0.79	0.56
POTS	13.07	52.19	19.44	13.93	0.13	0.11	−0.14	0.10

Table 3 (Contd.)

Site	λ	φ	V_e	V_n	σ_{Ve}	σ_{Vn}	Res_V_e	Res_V_n
SJDV	4.68	45.69	19.95	14.81	0.74	1.01	0.46	0.07
TIXI	128.87	71.52	16.44	−12.56	0.20	0.24	0.44	−0.06
UZHL	22.30	48.44	22.08	12.21	1.25	1.59	0.07	−0.28
WROC	17.06	50.93	20.54	13.67	2.20	2.44	−0.06	0.37
WSRT	6.60	52.73	17.98	15.05	0.15	0.15	−0.20	0.49
WTZR	12.88	48.95	20.60	14.17	0.13	0.11	0.33	0.32
WTZZ	12.88	48.95	20.48	13.71	1.59	2.00	0.21	−0.14
YAKT	129.68	61.87	18.28	−13.24	0.47	0.58	−0.44	−0.61
YEBE	−3.09	40.33	19.11	15.32	1.18	1.13	−0.16	0.02
ZECK	41.57	43.60	26.48	9.89	0.23	0.24	1.15	1.17
ZIMJ	7.47	46.69	19.72	13.98	1.38	1.67	−0.06	−0.49
ZIMM	7.47	46.69	20.67	14.52	0.15	0.15	0.89	0.05
bada	102.23	51.58	25.00	−7.03	1.16	0.84	0.01	−0.03
krab	92.79	55.81	24.42	−5.75	0.28	0.28	−0.62	−1.13
meta	24.38	60.08	18.85	11.79	0.73	0.55	−0.92	−0.35
NYAL_D	11.87	78.86	10.54	13.30	0.14	0.15	−0.61	−0.66
METS	24.40	60.05	20.21	11.58	0.15	0.13	0.44	−0.56
India (indi)								
DGAR	72.37	−7.22	46.38	30.45	0.23	0.13	−0.71	−0.84
IISC	77.57	12.94	41.34	33.43	0.20	0.12	0.64	0.64
cola	79.87	6.85	41.40	35.57	1.08	0.66	−1.85	2.21
North America (noam)								
ALGO	−78.07	45.76	−16.31	1.40	0.19	0.13	0.32	−0.59
AMC2	−104.52	38.62	−15.19	−6.79	0.28	0.25	−1.17	0.89
AOML	−80.16	25.58	−10.21	1.31	0.41	0.32	0.84	0.09
BARH	−68.22	44.20	−16.36	5.33	0.42	0.25	−0.55	−0.26
BAKE	−96.00	64.17	−19.29	−4.31	2.33	2.21	0.30	0.32
BRMU	−64.70	32.20	−12.01	7.21	0.81	0.73	0.49	0.36
CAGS	−75.81	45.39	−16.22	2.17	1.79	1.44	0.26	−0.66
DUBO	−95.87	50.07	−17.36	−4.73	0.23	0.22	−0.09	−0.14
EPRT	−66.99	44.72	−15.55	6.38	1.08	1.25	0.29	0.35
FLIN	−101.98	54.54	−17.52	−7.76	0.20	0.18	0.11	−0.98
GODE	−76.83	38.83	−14.69	2.91	0.20	0.15	0.19	0.46
HLFX	−63.61	44.49	−15.12	7.02	2.05	2.22	0.39	−0.21
HNPT	−76.13	38.40	−14.33	1.26	1.28	1.48	0.41	−1.44
MDO1	−104.01	30.51	−12.59	−7.00	0.22	0.17	−0.68	0.50
NAIN	−61.69	56.36	−16.47	9.24	1.77	2.42	1.13	1.35
NLIB	−91.57	41.58	−15.62	−2.58	0.21	0.16	−0.08	0.44
NRC1	−75.62	45.26	−16.16	2.73	0.21	0.15	0.28	−0.16
RCM6	−80.38	25.46	−9.78	1.77	1.26	0.86	1.23	0.64
SCH2	−66.83	54.65	−17.81	6.49	0.22	0.20	0.02	0.40
SOL1	−76.45	38.13	−14.69	2.79	0.64	0.40	−0.01	0.20
UNB1	−66.64	45.76	−16.18	6.29	1.08	1.40	−0.13	0.14
USN3	−77.07	38.73	−14.34	2.95	4.32	5.25	0.51	0.59
USNA	−76.48	38.80	−15.03	2.33	0.60	0.39	−0.17	−0.25
USNO	−77.07	38.73	−15.05	2.56	0.22	0.17	−0.19	0.20
WES2	−71.49	42.42	−15.76	3.78	0.19	0.13	−0.18	−0.62
WILL	−122.17	52.05	−14.38	−12.37	0.25	0.21	−0.01	0.96
YELL	−114.48	62.32	−16.81	−11.53	0.18	0.14	0.29	−0.55
Greb	−76.83	38.83	−14.54	2.44	2.96	1.77	0.34	−0.01
STJO_D	−52.68	47.40	−14.50	11.47	0.17	0.13	0.37	0.58
Nubia (nubi)								
ALEX	29.91	31.03	21.03	15.53	0.78	0.50	−1.16	−1.10
GMAS	−15.63	27.61	16.42	14.91	2.77	2.41	0.31	−1.29
GOUG	−9.88	−40.16	20.98	17.47	0.27	0.19	0.44	0.61
MAS1	−15.63	27.61	16.21	16.24	0.15	0.10	0.09	0.03
PHLW	31.34	29.70	22.46	17.34	0.61	0.39	−0.06	0.88
SUTH	20.81	−32.21	16.29	17.63	0.17	0.14	−0.41	0.20
SUTM	20.81	−32.21	16.45	18.29	0.81	0.76	−0.24	0.86
TGCV	−22.98	16.65	19.15	14.31	4.89	2.26	0.71	−0.83
YKRO	−5.24	6.83	21.50	16.52	0.66	0.32	0.11	−0.77
ZAMB	28.31	−15.33	18.20	16.81	0.74	0.40	−1.52	0.00
daka	−17.43	14.64	18.66	17.52	2.36	1.32	−0.69	1.54
hela	−5.67	−15.84	22.06	18.60	1.02	0.64	−0.39	1.35
tria	−12.31	−36.88	22.79	16.78	1.53	1.04	1.30	0.18
HRAO_D	27.71	−25.74	17.89	16.82	0.15	0.11	0.51	−0.05
NKLG_D	9.67	0.35	21.53	17.46	0.30	0.17	−0.54	−0.36

Table 3 (Contd.)

Site	λ	φ	V_e	V_n	σ_{Ve}	σ_{Vn}	Res_V_e	Res_V_n
South America (soam)								
BRAZ	−47.88	−15.85	−3.24	10.56	0.27	0.19	0.41	0.17
CHPI	−44.99	−22.55	−3.68	11.51	0.64	0.45	−0.15	1.06
CORD	−64.47	−31.36	−0.13	9.71	0.48	0.43	1.20	0.17
KOUR	−52.81	5.22	−4.67	10.69	0.24	0.16	−0.27	0.46
FORT	−38.43	−3.85	−4.08	10.28	0.21	0.15	0.14	−0.20
LPGS	−57.93	−34.73	−1.28	9.58	0.20	0.18	0.33	−0.38
ASC1_D	−14.41	−7.90	−5.44	9.25	0.21	0.13	−0.65	−0.21
Somalia (soma)								
MALI	40.19	−2.98	26.08	13.65	0.31	0.13	0.25	−0.24
MIR1	47.48	−18.68	19.62	10.68	4.16	1.52	−0.47	−1.27
RBAY	32.08	−28.63	16.15	15.99	0.42	0.30	−1.32	0.22
SEY1	55.48	−4.64	26.61	9.88	0.61	0.23	1.49	0.27
REUN_D	55.57	−21.08	18.52	9.98	0.41	0.22	−0.01	0.40

Sites in upper case are GPS-only sites, lower case are DORIS-only sites, and upper case ending by _D are co-located GPS–DORIS sites. λ, φ : longitude and latitude of sites in decimal degrees; V_e, V_n : ITRF2000 velocities in mm/year, σ_{Ve}, σ_{Vn}: velocity standard deviations; Res_V_e, Res_V_n : residual velocities with respect to the stable plate

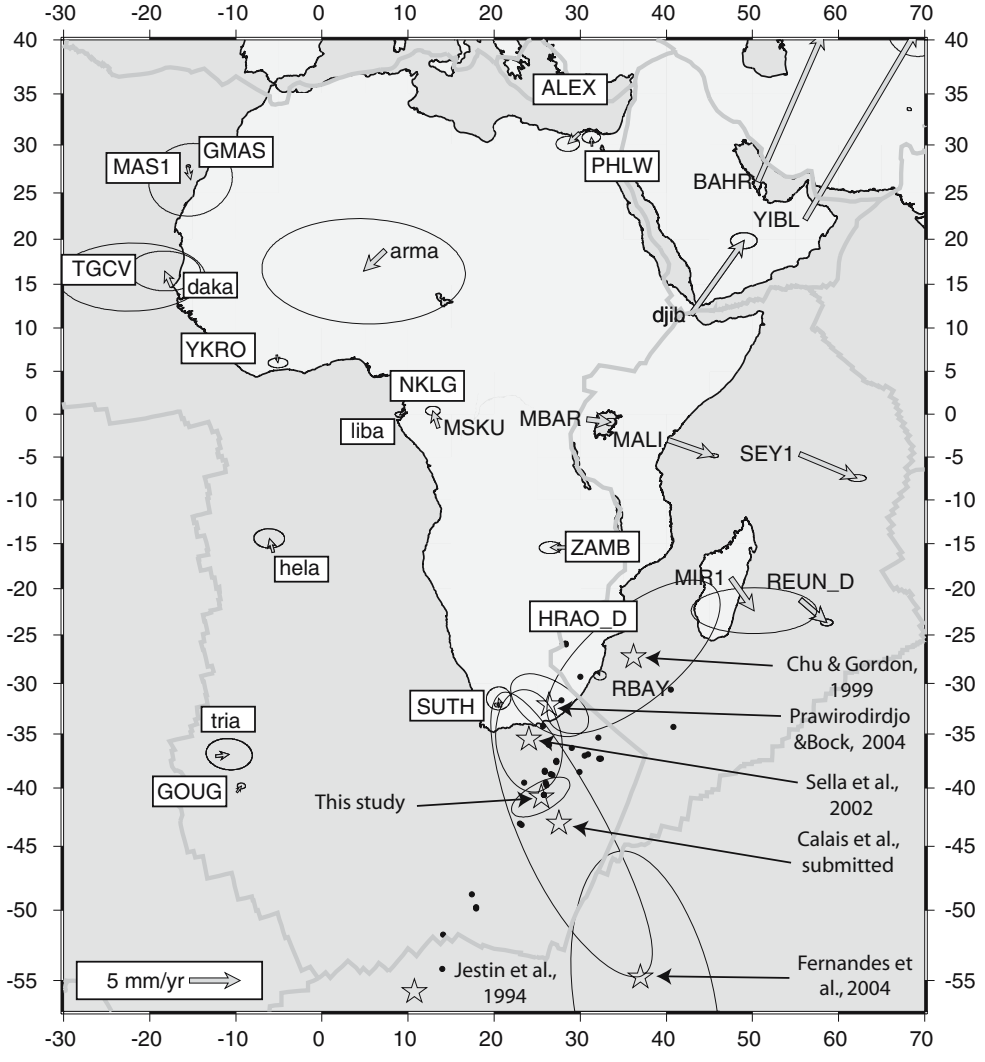

Fig. 5 GPS (*upper case*) and DORIS (*lower case*) and GPS–DORIS co-located sites (*upper case ending with _D*) velocities relative to Nubia. Nubia is defined using the sites in *white rectangles*. *Stars* indicate Euler pole for Somalia/Nubia relative motion with one-sigma error ellipse. *Black dots* indicate locations of Nubia/Somalia Euler pole for our precision simulation (see text). Velocities are relative to Nubia. Velocity ellipse errors are given at a 95% confidence level. *Grey lines* are plate boundaries from Bird (2003)

ranges from 4.7 to 6.7 mm/year for all the subset of sites chosen, with a direction changing between N90°E and N108°E. Our best estimate uses all five sites and predicts a 5.5 mm/year opening rate at an azimuth of N105°E.

Our estimate differs from previously published geodetic results. For instance, our best estimate of opening rate is 25% slower than the value predicted by Sella et al. (2002). The location of the Euler pole predicts different tectonic regimes along the plate boundary south of South Africa. While Fernandes et al.'s (2004) results would predict mainly EW extension, our Euler pole mainly predicts right-lateral shear with a very small amount of relative motion (<1.5 mm/year) that correlates with the lack of seismicity or any major tectonic structure.

Differences may stem from the length of the time-series used in the analysis, the version of the global reference frame used and its implementation and the choice of sites used to define stable plates. Here, it is likely that the major difference is due to sites REUN and MIR1 on the Somalia plate. Our estimate is also significantly different from the estimate based on magnetic anomaly analysis and averaging the opening rates along southwestern Indian Ridge zone over 3.16 Myear (Chu and Gordon 1999; Lemaux et al. 2002; Horner-Johnson et al. 2005). Horner-Johnson et al. (2005), for instance, predict an opening rate of 8.3 ± 1.9 mm/year at an azimuth of N121°E in Afar.

While our best estimate predicts a 30% slower opening rate, it is consistent with estimates derived from tectonic observation and local geodetic measurements. For instance, Ebinger (1989) proposed an upper bound of 20–30 km of finite extension since 5 Ma, leading to a maximum opening rate of 5–6 mm/year at latitude 9°N (Jestin et al. 1994). Moreover, local GPS and satellite laser ranging (SLR) measurements indicated an opening rate of 4.0–4.5 ± 1 mm/year at latitude ∼ 8.5°N in Ethiopia (Bilham et al. 1999; Bendick et al. 2006), consistent with our estimate. The difference between our model and the model based on magnetic anomalies analysis may arise from recent changes in the relative plate kinematics or deformation of oceanic areas of the Somalia and Nubia plates south of Africa (Horner-Johnson et al. 2005).

6 Relative plate motion of surrounding plates

In the following, we estimate rotation vectors for plates surrounding Nubia and Somalia and assess the impact of splitting Africa into two plates by comparing opening rates predicted along the Indian Ocean and southern Atlantic ridges to the values predicted by NUVEL-1A (DeMets et al. 1990, 1994) that considers Africa as a single rigid plate, but includes data both in the southern Atlantic and Indian oceans (Figs. 6, 7). Table 4 shows our rotation vector estimates expressed in the ITRF2000, and Table 5 compares the relative plate motion versus the prediction of Prawirodidjo and Bock (2004), Sella et al. (2002) and recent plate kinematics models in the area.

6.1 Antarctica/Nubia and Antarctica/Somalia

Our estimate of the Antarctica rotation vector includes ten sites, including two independent DORIS sites and a good geographic coverage of the Antarctica plate. The WRMS of residual velocities is 0.6 mm/year, showing a high level of rigidity for this plate and thus indicating a very small influence of current glacial rebound, at least on the horizontal velocities. Compared to NUVEL-1A, opening rate and direction agree within 1 mm/year and 5° in direction along the plate boundary between longitudes 0° and 30°E. A larger difference is noted further east on the part of the ridge corresponding to the Antarctica/Somalia boundary, with differences increasing eastward up to 4 mm/year at the Somalia/Antarctica/Australia triple junction.

Interestingly, our model predicts a steadily increasing rate as one moves eastward. The slow change, rather than an abrupt change, explains why the location of the boundary between Nubia and Somalia is difficult to constrain using magnetic anomalies along the ridge separating Nubia–Somalia from Antarctica. Our Euler poles are in very good agreement with Sella et al. (2002) for the Antarctica/Somalia relative motion and with Prawirodidjo and Bock (2004) for the Antarctica/Nubia motion.

6.2 Nubia/South America and Nubia/North America

Plate motion for South America is derived using seven sites located outside well-known deforming areas like the Andes and including the site located on the Ascension Island (ASC1) in the southern Atlantic Ocean. Here again, the WRMS of residual velocities is the smallest found for all plates studied here (0.5 mm/year), showing excellent agreement with the rigid-plate hypothesis.

For North America, we used 29 sites sampling the plate east of the Rocky Mountain Range to avoid any tectonics-based deformation. We find a WRMS of horizontal velocities of 0.6 mm/year, similar to values found by Calais et al. (2005). Compared to NUVEL-1A, we find opening rates 15% slower and a significantly different direction of extension along the South America/Nubia diverging boundary, confirming previous results from Sella et al. (2002).

This difference has been interpreted as a deceleration of the spreading rate in the southern Atlantic since ∼25 Myear (Cande and Kent 1992). We also notice that we find a very slow transition in both magnitude and direction of extension as one moves from the Nubia/South America to Nubia/North America boundary. This result agrees with a very small relative motion between the North and South America plates.

6.3 Nubia/Eurasia

The Nubia/Eurasia relative plate motion provides the kinematic boundary conditions to the Mediterranean system. Previous studies have shown that the present-day convergence is 30–50% slower and more oblique than the prediction of

Table 4 Estimated ITRF2000 Euler poles for the Somalia and Nubia and surrounding plates

Plate	λ	φ	Ω	σ_1	σ_2	azim	σ_Ω	#	WRMS	σ_0
anta	−128.51	60.41	0.22	0.22	0.16	−107	0.002	10	0.57	2.46
arab	−26.80	52.99	0.43	2.90	0.14	26	0.011	2	3.53	6.72
arab	−26.80	52.99	0.43	2.90	0.14	26	0.011	2	3.53	6.72
aust	38.18	32.44	0.62	0.11	0.05	−102	0.001	18	0.61	3.00
eura	−104.46	55.45	0.25	0.19	0.07	−131	0.001	46	0.58	2.58
indi	12.15	51.43	0.52	0.73	0.11	−78	0.003	4	1.53	4.72
noam	−83.43	−5.51	0.19	0.39	0.11	−2	0.001	29	0.56	2.04
nubi	−81.11	51.07	0.25	0.26	0.13	−34	0.001	16	0.76	1.65
soam	−129.96	−21.86	0.10	1.08	0.48	−56	0.001	7	0.53	2.06
soma	−95.76	53.11	0.30	0.78	0.23	156	0.004	5	0.79	1.91

λ, φ : latitude and longitude of the Euler pole in decimal degrees; Ω : angular velocity in degrees per Myear; σ_1, σ_2: one-sigma lengths in degrees of the semi-major and semi-minor axes of the Euler pole ellipse; azim : azimuth of the semi-major ellipse axis in degrees clockwise from north; σ_Ω: one-sigma error on Ω ;# : number of sites used in estimation; WRMS: weighted root mean square of the residual velocities; σ_0: a posteriori variance factor (χ^2 / degrees of freedom). The plate acronyms are defined in Table 3

Table 5 Relative plate Euler poles (this study) versus recently published models

Pair of plates	λ	φ	Ω	σ_1	σ_2	azim	σ_Ω
nubi-soma	25.46	−40.78	0.06	2.86	1.24	−120	0.005
PB2004	26.37	−32.16	0.10	4.29	2.41	123	0.021
F2004	36.97	−54.76	0.07	9.50	4.60	169	0.009
S2002	24.02	−35.49	0.08	4.90	3.10	171	0.005
CG1999	36.20	−27.3	0.09	6.90	5.50	38	0.004
anta-soma	117.60	−24.77	0.12	2.40	1.18	33	0.003
S2002	115.25	−28.17	0.12	5.20	3.10	16	0.007
arab-soma	14.30	21.64	0.27	2.82	0.80	50	0.021
PB2004	27.24	20.13	0.46	0.78	0.33	42	0.034
S2002	28.62	21.06	0.44	1.80	1.00	55	0.029
indi-soma	36.40	21.88	0.45	0.67	0.38	−147	0.007
PB2004	−5.80	16.72	0.32	15.32	1.03	6	0.032
S2002	19.46	22.78	0.36	13.1	0.90	89	0.040
aust-soma	49.52	7.92	0.66	0.24	0.13	−1.5	0.005
PB2004	47.59	7.10	0.70	0.85	0.16	149	0.020
S2002	48.55	9.31	0.67	1.20	0.40	−57	0.004
nubi-anta	−38.72	3.94	0.12	1.14	0.50	−80	0.001
PB2004	−39.50	−3.48	0.11	3.82	1.09	74	0.010
S2002	−31.90	3.25	0.13	6.80	2.70	16	0.006
nubi-soam	−45.23	62.84	0.27	0.45	0.23	−60	0.001
PB2004	−43.25	62.04	0.27	1.63	0.88	140	0.007
S2002	24.02	−35.49	0.08	4.90	3.10	−19	0.005
noam-nubi	−94.99	−81.50	0.22	0.35	0.31	−8	0.001
PB2004	87.592	−78.93	0.32	15.32	1.03	6	0.032
S2002	−75.23	−77.90	0.21	2.00	1.20	64	0.004
nubi-eura	−20.43	−5.03	−0.06	1.05	0.69	56	0.001
PB2004	−22.10	20.10	0.05	5.05	0.95	114	0.005
S2002	−20.01	18.23	0.06	9.50	3.70	−17	0.005
MC2003	−21.80	−0.95	0.06	4.80[a]	4.30[a]	NA	0.005
arab-nubi	32.39	31.66	0.50	4.98	0.20	−59	0.14
S2002	29.55	31.26	0.40	1.80	1.30	275	0.03
MC2003	25.70	30.50	0.37	1.00[a]	2.30[a]	NA	0.040
V2006	20.29	31.64	0.31	2.50	1.10	290	0.018
arab-soma	31.69	25.07	0.52	4.78	0.43	29.1	0.141
S2002	28.62	21.06	0.44	1.80	1.00	55	0.029
V2006	25.49	20.07	0.36	2.30	1.20	286	0.026

The first plate rotates counterclockwise relative to the second plate around the Euler pole; PB2004 = Prawirodidjo and Bock (2004), F2004 = Fernandes et al. (2004), S2002 = Sella et al. (2002), CG1999 = Chu and Gordon (1999), MC2003 = McClusky et al. (2003), V2006 = Vigny et al. (2006). λ, φ : latitude and longitude of the Euler pole in decimal degree; Ω : angular velocity in degrees per Myear; σ_1, σ_2: one-sigma lengths in degrees of the semi-major and semi-minor axes of the Euler pole ellipse; azim : azimuth of the semi-major ellipse axis in degrees clockwise from north; σ_Ω: one-sigma error on Ω . The plate acronyms are defined in Table 3.

[a]Values indicate formal error of the longitude and latitude of the Euler pole

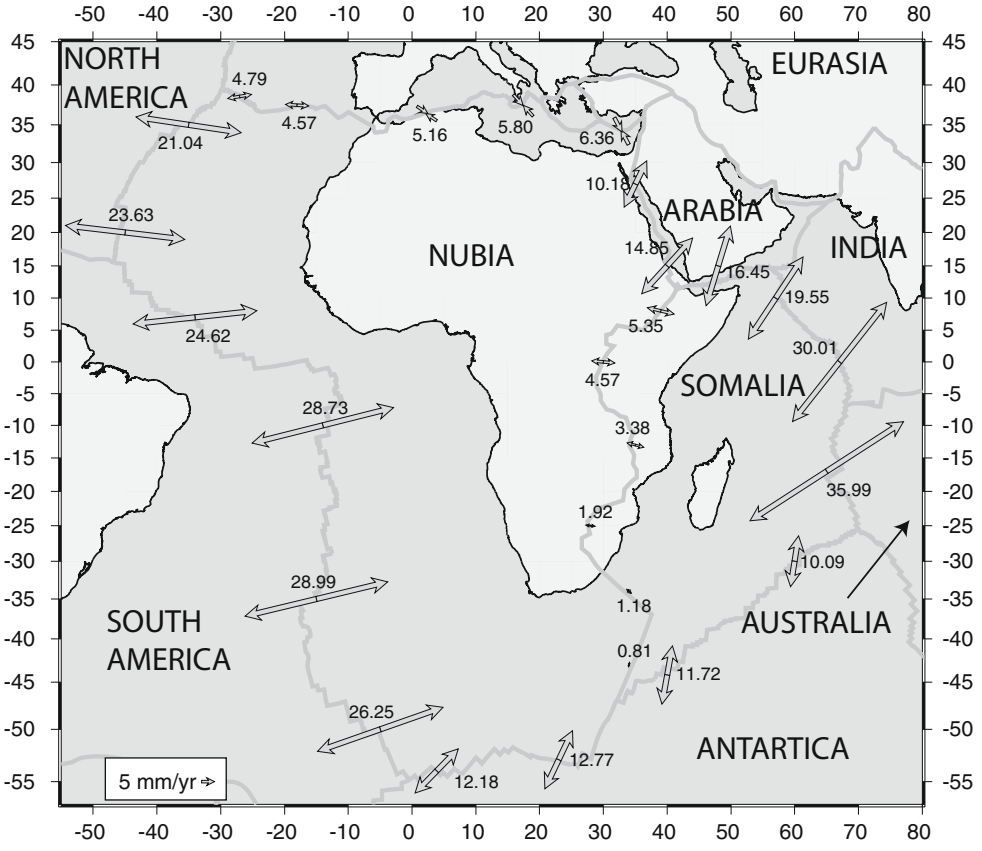

Fig. 6 Relative plate motion predicted at plate boundaries (this study). Numerical values are in mm/year

NUVEL-1A (see Nocquet and Calais 2004 for a review of different models) with a pole located several thousands of kilometres south of the NUVEL-1A proposed value. Our new analysis, including two well-determined permanent sites in Egypt, provides good constraints on the Europe/Nubia convergence rate along the Mediterranean and rules out the north-eastward convergence of Nubia as proposed recently by Babbucci et al. (2004).

We find a maximum convergence rate of 7 mm/year at the easternmost part of the Mediterranean, 5.8 mm/year in Central Mediterranean, 5.2 mm/year along the Maghrebides in Northern Africa, 4.6 mm/year of right lateral motion along the Gloria fault and 4.8 mm/year of extension along the Terceira ridge. Our estimate significantly differs from Prawirodidjo and Bock (2004) and Sella et al. (2002), but is closer to McClusky et al. (2003).

We suspect that the different estimates obtained by the different authors stem not only from the choice of sites used to define the Nubia kinematics, but also the choice of sites used to define Eurasia. Indeed, in previous studies, most of the high-quality geodetic sites were only available over Europe, at least west of the Ural mountain range. The present study includes as many sites as possible in the eastern part of the continent (outside well-known deforming areas in Asia). We note that including these sites does not increase the WRMS of the residual velocity (0.6 mm/year) or the reduced χ^2 (1.58). We therefore believe that our definition of stable Eurasia is optimal in terms of geometry and selection of sites.

6.4 Nubia/Arabia and Somalia/Arabia

With only two sites on the Arabia plate, our angular velocity vector is poorly constrained. However, our prediction for the Nubia/Arabia motion agrees with more robust estimate from Vigny et al. (2006), with opening rates in the Red Sea ranging from 8 mm/year in its northern part to 15 mm/year in its southern part. Although these estimates are not significantly different from NUVEL-1A predictions, geodetically based opening rates in the Red Sea are ∼15% slower than Chu and Gordon's (1999) estimate based on magnetic anomalies over the last 3 Myear. This result, together with analysis carried out by Calais et al. (2003) for the Eurasia/Nubia convergence rate, may reflect a deceleration of the convergence rate along the whole Alpine–Himalayan collision belt, as suggested by Vigny et al. (2006).

6.5 Somalia/India and Somalia/Australia

With only four sites available to estimate the kinematics of the India plate with a WRMS of 1.5 mm/year and a reduced χ^2 of 4.7, the kinematics of India has yet to be accurately

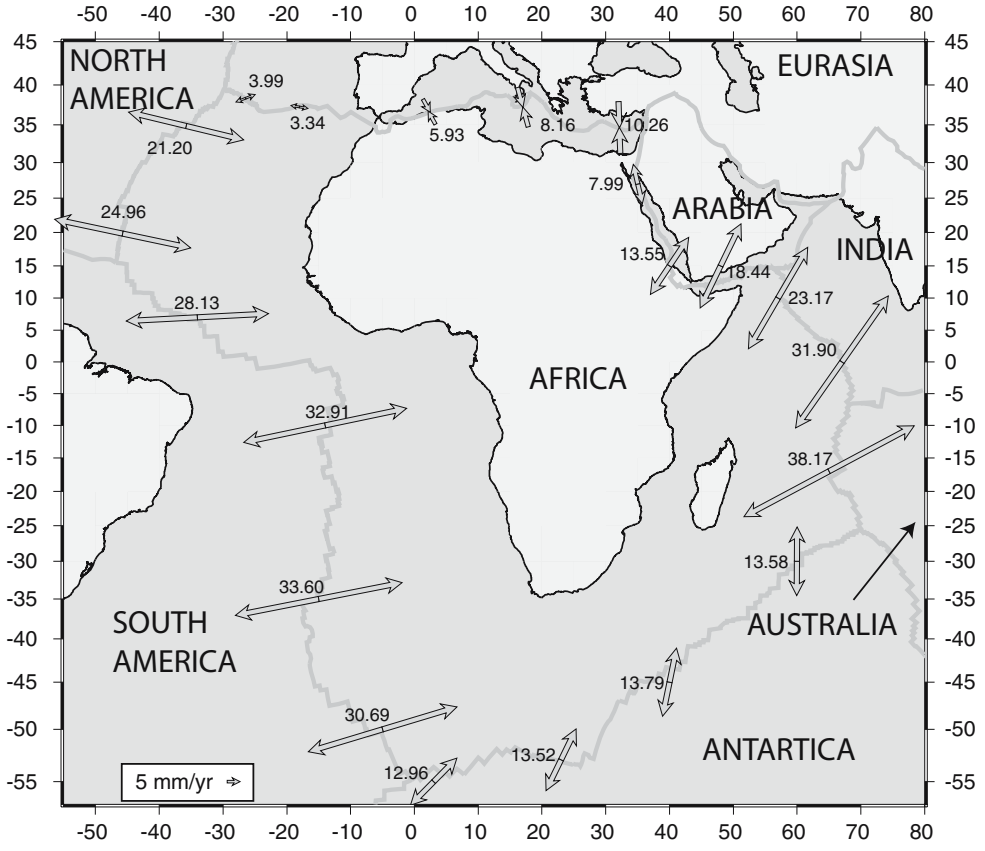

Fig. 7 Relative plate motion predicted at plate boundaries by NUVEL1A (DeMets et al. 1990, 1994). Numerical values are in mm/year

determined. Moreover, MALD (Maldives islands) shows a 6 mm/year residual velocity relatively to an India-fixed reference frame, and has therefore been rejected in the rotation vector calculation. Our estimate of the Somalia/India motion is 2 mm/year slower than the values predicted by NUVEL-1A and our pole differs from the model of Prawirodidjo and Bock (2004) and Sella et al. (2002). However, our model shows a very good agreement with rates recently derived from magnetic anomalies over the last 4 Myear (DeMets et al. 2005).

The Australia plate, with 18 sites, is well determined and our estimate agrees well with prediction from Prawirodidjo and Bock (2004) and Sella et al. (2002). Our model indicates 2 mm/year (6%) slower opening rate along the Indian ridge than values predicted by NUVEL-1A. The 2 mm/year roughly corresponds to the motion of Somalia with respect to Nubia and therefore possibly reflects the bias of NUVEL-1A due to the fact that NUVEL-1A considers Africa as a single non-deforming plate. Alternatively, more recent models include a Capricorn plate, which may have a slight motion relative to the Australian plate. Our estimate is again 2 mm/year slower than the estimate derived by DeMets et al. (2005) from magnetic anomalies. This discrepancy may reflect a slow relative motion between the Capricorn and Australian plates.

7 Conclusions

Our analysis of DORIS time-series shows that a model combining white noise and flicker noise best explains the noise content of the time-series. While Williams and Willis (2006) find that the model using only white noise underestimates the velocity uncertainties by a factor of about three, a rigorous combination with two independent global GPS solutions indicates that a factor of about two still needs to be applied to the DORIS variance solution in order to make the residuals obtained in the combination consistent with velocities and position uncertainties.

The combination indicates that DORIS horizontal velocities have an average accuracy of 3 mm/year. Best-determined sites (those with longer data spans) show accuracy of the order of 1 mm/year, indicated by standard deviation derived from the combination, comparison with GPS velocities for co-located sites and the residual velocities in the rigid plate motion estimation. With such accuracy, the DORIS solution can contribute to the determination of plate kinematics on plates poorly determined using GPS-only solutions.

More specifically, we find that the variance of the Nubia angular velocity vector is improved by 15% when DORIS sites are included in the estimation. Moreover, DORIS sites

clearly confirm that sites located on the oceanic lithosphere and sites located on the continental lithosphere of the Nubia plate are moving rigidly together, a question that had been raised when the plate tectonics theory was formulated.

Using our improved estimate of the Nubia kinematics, we use five sites to determine the kinematics of Somalia and provide robust estimate of the Somalia/Nubia relative motion. We find that the maximum opening rate in northern Ethiopia is 4.7–6.7 mm/year. We then derive relative motion of Nubia and Somalia relatively to their neighbouring plates. The opening rate in the southern Atlantic is found to be 15% slower than the values predicted by the NUVEL-1A model, as found previously by Sella et al. (2002).

In the Mediterranean, while most geodetic models find slower and more westward oblique convergence, the discrepancies between geodetic models is still of the order of 2 mm/year, a value that still prevents accurate tectonic interpretation in slowly converging areas. The observed differences with NUVEL-1A in oceanic opening rates are likely to be partly the consequence of the fact that NUVEL-1A considers Africa as a single non-deforming plate and therefore neglects the eastward motion of Somalia relative to Nubia.

Acknowledgments We are grateful to the Agence pour la Sécurité de la Navigation Aérienne en Afrique et à Madagascar (ASECNA) for allowing us to use their GPS campaign data. We thank C. DeMets, W. Featherstone and two anonymous reviewers for their corrections that help to improve the manuscript. We thank Z. Altamimi for providing us the CATREF software and for advice at the combination step. Finally, we thank all individuals and institutions contributing to the IGS for making their high-quality data and analysis results publicly available. Part of this work was carried out at the Jet Propulsion Laboratory, California Institute of Technology, under a contract with the National Aeronautics and Space Administration. This is Geosciences Azur contribution 858.

References

Altamimi Z, Sillard P, Boucher C (2002) ITRF2000, a new release of the International Terrestrial Reference Frame for Earth science applications. J Geophys Res 107(B10):2214. DOI 10.1029/2001JB000561

Altamimi Z, Colillieux X, Boucher C (2006) DORIS contribution to ITRF2005. J Geod (this issue)

Argus DF, Heflin MB (1995) Plate motion and crustal deformation estimated with geodetic data from the Global Positioning System. Geophys Res Lett 22(15):1973–1976. DOI 10.1029/95GL02006

Babbucci D, Tamburelli C, Vitil M, Mantovani E, Albarello D, D'Onza Cenni1 F, Mugnaioli E (2004) Relative motion of the Adriatic with respect to the confining plates: seismological and geodetic constraints. Geophys J Int 159(2):765–775. DOI 10.1111/j.1365-246X.2004.02403

Bendick R, McClusky S, Bilham R, Asfaw L, Klemperer S (2006) Distributed Nubia–Somalia relative motion and dike intrusion in the Main Ethiopian Rift. Geophys J Int 165(1):303–311. DOI 10.1111/j.1365-246X.2006.02904.x

Beutler G, Rothacher M, Schaer S, Springer TA, Kouba J, Neilan RE (1999) The International GPS Service (IGS), an interdisciplinary service in support of Earth Sciences. In: Dow J, Beutler G (eds) Adv Space Res 23(4):631–653

Bilham R, Bendick R, Larson K, Mohr P, Braun J, Tesfaye S, Asfaw L (1999) Secular and tidal strain across the main Ethiopian rift Geophys Res Lett 26(18):2789–2792. DOI 0.1029/1998GL005315

Bird P (2003) An updated digital model of plate boundaries. Geochem Geophys Geosyst 4(3):1027. DOI 10.1029/2001GC000252

Calais E, DeMets C, Nocquet JM (2003) Evidence for a post-3.16 Ma change in Nubia–Eurasia–North America plate motions. Earth Planet Sci Lett 216(1–2):81–92. DOI 10.1016/S0012-821X(03)00482-5

Calais E, Mattioli G, DeMets C, Nocquet J-M, Stein S, Newman A, Rydelek P (2005) Tectonic strain in plate interiors? (Reply). Nature 438(7070):E9–E10. DOI 10.1038/nature04429

Calais E, Ebinger C, Hartnady C, Nocquet JM (2006) Kinematics of the East African rift from GPS and earthquake slip vector data. Geological Society of London, Special volume on East African rift

Cande SC, Kent DV (1992) A new geomagnetic polarity time scale for the Late Cretaceous Cenozoic. J Geophys Res 97(B10):13917–13951. DOI 10.1029/92JB01202

Christodoulidis DC, Smith DE, Kolenkiewicz R, Klosko SM, Torrence MH, Dunn PJ (1985) Observing tectonic plate motion and deformation from Satellite Laser Ranging. J Geophys Res 90(B11):9249–9263

Chu D, Gordon RG (1999) Evidence for motion between Nubia and Somalia along the Southwest Indian ridge. Nature 398(6722):64–67. DOI 10.1038/18014

Cretaux JF, Soudarin L, Cazenave A, Bouille F (1998) Present-day tectonic plate motions and crustal deformations from the DORIS space system. J Geophys Res 103(B12):30167–30181. DOI 10.1029/98JB02239

DeMets C (1995) A reappraisal of sea floor spreading lineations in the Gulf of California: implications for the transfer of Baja California to the pacific plate and estimates of Pacific–North America motion. Geophys Res Lett 22(24):3545–3548. DOI 10.1029/95GL03323

DeMets C, Gordon RG, Argus DF, Stein S (1990) Current plate motions. Geophys J Int 101(2):425–478

DeMets C, Gordon RG, Argus DF, Stein S (1994) Effect of recent revisions to the geomagnetic reversal time-scale on estimates of current plate motions. Geophys Res Lett 21(20):2191–2194. DOI 10.1029/94GL02118

DeMets C, Gordon RG, Royer J-Y (2005) Motion between the Indian, Capricorn and Somalian plates since 20 Ma: implications for the timing and magnitude of distributed lithospheric deformation in the equatorial Indian ocean. Geophys J Int 161(2):445–468. DOI 10.1111/j.1365–246X.2005.0298.x

Eanes RJ, Schuler A (1999) An improved global ocean tide model from TOPEX/Poseidon altimetry: CSR4.O. In: EGS, 24th general assembly, The Hague (NL)

Ebinger C (1989) Tectonic development of the western branch of the East African rift system. Geol Soc Am Bull 101:885–903

Fagard H (2006) 20 years of evolution of the DORIS network, from its initial deployment. J Geod (this issue)

Ferland R, Kouba J, Hutchison D (2000) Analysis methodology and recent results of the IGS network combination. Earth Planet Space 52(11):953–957

Fernandes RMS, Ambrosius BAC, Noomen R, Bastos L, Combrinck L, Miranda JM, Spakman W (2004) Angular velocities of Nubia and Somalia from continuous GPS data: implications on present-day relative kinematics. Earth Planet Sci Lett 222(1):197–208. DOI 10.1016/j.epsl.2004.02.008

Gordon RG (1995) Plate motions, crustal and lithospheric mobility, and paleomagnetism: Prospective viewpoint. J. Geophys Res 100(B12):24367. DOI 10.1029/95JB01912

Heflin M, Bertiger W, Blewitt G, Freedman A, Hurst K, Lichten S, Lindqwister U, Vigue Y, Webb F, Yunck T, Zumberge J (1992) Global geodesy using GPS without fiducial sites. Geophys Res Lett 19(2):131–134. DOI 10.1029/91GL02983

Herring TA, Shapiro II, Clark TA, Ryan JW, Schupler BR, Knight CA, Lundqvist G, Shaffer DB, Vandenberg NR, Corey BE, Hinteregger HF, Roggers AEE, Webber JC, Whitney AR, Elgered G, Ronnang BO, Davis JL (1986) Geodesy by radio interferometry: evidence for contemporary plate motion. J Geophys Res 91(B8): 8341–8347

Horner-Johnson BC, Gordon RG, Cowles SM, Argus DF (2005) The angular velocity of Nubia relative to Somalia and thelocation

of the Nubia–Somalia–Antarctica triple junction. Geophys J Int 162(1):221–238. DOI 10.1111/j.1365-246X.2005.02608
Jestin FP, Huchon JM, Gaulier (1994) The Somali plate and the East African Rift system: present-day kinematics. Geophys J Int 116:637–654
King RW, Bock Y (2005) Documentation for the GAMIT GPS software analysis, release 10.20. MIT, Cambridge
Kreemer C, Holt WE, Haines AJ (2003) An integrated global model of present-day plate motions and plate boundary deformation. Geophys J Int 154(1):8–34. DOI 10.1046/j.1365-246X.2003.01917.x
Larson KM, Freymueller JT, Philipsen E (1997) Global plate velocities from the global positioning system. J Geophys Res 102(B5):9961–9981. DOI 10.1029/97JB00514
Lemaux JII, Gordon RG, Royer JY (2002) Location of the Nubia–Somalia boundary along the Southwest Indian ridge. Geology 30(4):339–342
Le Pichon X (1968) Sea floor spreading and continental drift. J Geophys Res 73:3661–3697
Mao AL, Harrison CGA, Dixon TH (1999) Noise in GPS coordinate time series. J Geophys Res 104(B2):2797–2816. DOI 10.1029/1998JB900033
McCarthy DD, Petit G (2004) IERS Conventions 2003, IERS Tech Note 32, Frankfurt am Main: Verlag des Bundesamts für Kartographie und Geodäsie, 127 pp.
McClusky S, Reilinger R, Mahmoud S, Ben Sari D, Tealeb A (2003) GPS constraints on Africa (Nubia) and Arabia plate motions. Geophys J Int155(1):126–138. DOI 10.1046/j.1365-246X.2003.02023
McKenzie DP, Parker RL (1967) The North Pacific: an example of tectonics on a sphere. Nature 216:1276–1280
Moore AW, Neilan RE (2005) The International GPS Service tracking network, enabling diverse studies and projects through international cooperation. J Geodyn 40(4–5):461–469. DOI 10.1016/j.jog.2005.10.009
Morel L, Willis P (2002) Parameter sensitivity of TOPEX orbit and derived mean sea level to DORIS station coordinates. Adv Space Res 30(2):255–263. DOI 10.1016/S0273-1177(02)00293-4
Morgan WJ (1968) Rises, trenches, great faults, and crustal blocks. J Geophys Res 73:1959–1982
Nerem RS, Mitchum GT (2002) Estimates of vertical crustal motion derived from differences of TOPEX/Poseidon and tide gauges sea level measurements. Geophys Res Lett 29(19):1934. DOI 10.1029/2002GL015037
Nocquet J-M, Calais E (2004) Geodetic measurements of crustal deformation in the Western Mediterranean and Europe. In: Nocquet J.-M, Calais E (eds) Pure and Appl Geophys 161(3):661–668. DOI 10.1007/s00024-003-2468-z
Nocquet J-M, Calais E, Altamimi Z, Sillard P, Boucher C (2001) Intraplate deformation in western Europe deduced from an analysis of the ITRF97 velocity field. J Geophys Res 106(B6):11239. DOI 10.1029/2000JB900410
Nocquet J-M, Calais E, Parsons B (2005) Geodetic constraints on glacial isostatic adjustment in Europe. Geophys Res Lett 32(6):L06308. DOI 10.1029/2004GL022174
Prawirodirdjo L, Bock Y (2004) Instantaneous global plate motion from 12 years of continuous GPS observations. J Geophys Res 109(B8):B08405. DOI 10.1029/2003JB002944
Sella GF, Dixon TH, Mao A (2002) REVEL: a model for recent plate velocities from space geodesy. J Geophys Res 107(B4):2081. DOI 10.1029/2000JB000033
Sillard P, Boucher C (2001) A review of algebraic constraints in Terrestrial Reference Frame datum definition. J Geod 75(2–3):63–73. DOI 10.1007/s001900100166
Soudarin L (2005) Discussions DORIS station discontinuities on IDS Analysis Forum. http://listes.cls.fr/wws/info/ids.analysis.forum
Soudarin L, Cretaux JF, Cazenave A (1999) Vertical crustal motions from the DORIS space-geodesy system. Geophys Res Lett 26(9):1207–1210. DOI 10.1029/1999GL900215
Tapley BD, Bettadpur S, Ries JC, Thompson PF, Watkins MM (2004) GRACE measurements of mass variability in the Earth system. Science 305(5683):503–505. DOI 10.1126/science.1099192
Tavernier G, Fagard H, Feissel-Vernier M, Lemoine F, Noll C, Ries J, Soudarin L, Willis P (2005) The International DORIS Service (IDS). Adv Space Res 36(3):333–341. DOI 10.1016/j.asr.2005.03.102
Vigny C, Huchon P, Ruegg J-C, Khanbari K, Asfaw LM (2006) Confirmation of Arabia plate slow motion by new GPS data in Yemen. J Geophys Res 111(B02402). DOI 10.1029/2004JB003229
Webb F, Zumberge J (eds) (1995) An introduction to GIPSY/OASIS II, Rep. JPLM D-11088. Jet Propulsion Lab, Pasadena
Williams SDP (2003) The effect of coloured noise on the uncertainties of rates estimated from geodetic time series. J Geod 76(9–10):483–494. DOI 10.1007/s00190-002-0283-4
Williams SDP, Willis P (2006) Error analysis of weekly station coordinates in the DORIS network. J Geod (this issue)
Williams SDP, Bock Y, Fang P, Jamason P, Nikolaidis RM, Prawirodirdjo L, Miller M, Johnson DJ (2004) Error analysis of continuous GPS position time series. J Geophys Res 109(B3):B03412. DOI 10.1029/2003JB002741
Willis P, Heflin MB (2004) External validation of the GRACE GGM01C gravity field using GPS and DORIS positioning results. Geophys Res Lett 31(13):L13616. DOI 10.1029/2004GL020038
Willis P, Ries JC (2005) Defining a DORIS core network for Jason-1 precise orbit determination. J Geod 79(6–7):370–378. DOI 10.1007/s00190-005-0475-9
Willis P, Haines B, Bar-Sever Y, Bertiger W, Muellerschoen R, Kuang D, Desai S (2003) TOPEX/Jason combined GPS/DORIS orbit determination in the tandem phase. Adv Space Res 31(8):1941–1946. DOI 10.1016/S0273-1177(03)00156-X
Willis P, Haines B, Berthias JP, Sengenes P, Le Mouel JL (2004) Behavior of the DORIS/Jason oscillator over the South Atlantic Anomaly. CR Geosci 336(9):839–846. DOI 10.1016/j.crte.2004/01.004
Willis P, Boucher C, Fagard H, Altamimi Z (2005a) Geodetic applications of the DORIS system at the French Institut Geographique National. CR Geosci 337(7):653–662. DOI 10.1016/j.crte.2005.03.002
Willis P, Soudarin L, Fagard H, Ries J, Noomen R (2005b) IDS recommendations for ITRF2004, version 1.0, 15 November 2005. IDS Tech Report
Willis P, Jayles C, Bar-Sever YE (2006a) DORIS from orbit determination for altimeter missions to geodesy. CR Geosci. DOI 10.1016/j.crte.2005.11.013
Willis P, Berthias JP, Bar-Sever YE (2006b) Systematic errors in the Z-geocenter derived using satellite tracking data, a case study from SPOT-4 DORIS data in 1998. J Geod 79(10–11):567–572. DOI 10.1007/s00190-005-0013-9
Wilson JT (1965) A new class of faults and their bearing on continental drift. Nature 207:343–347
Zhang J, Bock Y, Jonhson H, Fang P, Williams S, Genrich J, Wdowinski S, Behr J (1997) Southern California permanent GPS geodetic array, error analysis of daily position estimates and site velocities. J Geophys Res 102(B8):18035–18055. DOI 10.1029/97JB01380